Dynamics of Ultrahigh Molecular Rydbergs in Weak Electric Fields

M. Bixon* and Joshua Jortner*

School of Chemistry, Tel Aviv University, Ramat Aviv, Tel Aviv 69978, Israel

Received: January 10, 1995⊗

In this paper we explore the dynamics of the mixed Stark manifold of ultrahigh Rydberg states (principal quantum number $n = 50-250$) of the large molecules interrogated by time-resolved ZEKE (zero-electron kinetic energy) spectroscopy. We pursue the formal analogy between the coupling, accessibility, and decay of ultrahigh Rydbergs in an external weak ($F = 0.01-1.0$ V/cm) electric field and intramolecular (interstate and intrastate) relaxation in a bound level structure. The effective Hamiltonian formalism with several doorway and escape states was advanced to treat the dynamics. The theory accounts for the dilution effect, i.e., the dramatic lengthening of the lifetimes of ultrahigh Rydbergs, relative to that expected on the basis of the n^{-3} scaling law for the decay widths. Model calculations for the field-induced (l) mixing reveal that the Rydberg time-resolved population probability is characterized by two distinct ($\sim$ns and $\sim\mu$s) time scales. To date, long time-resolved (10 μs−100 ns time scales) nonexponential decay of ZEKE Rydbergs was experimentally documented, in accord with our analysis. The predicted existence of the short decay times (1−10 ns) was not yet subjected to an experimental test. Next, we extend the model calculations to treat the mixing of several n manifolds, demonstrating that in the strong mixing limit the overall features of the temporal decay are similar to that of a single n manifold.

I. Intramolecular Dynamics of High Rydbergs

The understanding of radiationless relaxation in electronically excited states of atoms and molecules dates back to the genesis of quantum mechanics, having its origins in the exploration of "reactive" nonradiative processes involving the decay of a metastable state(s) to a continuum, i.e., molecular predissociation[1,2] and atomic autoionization.[3,4] Indeed, the pioneering studies in the 1920s of molecular predissociation[1] provided the experimental verification of the Heisenberg time−energy uncertainty relation, with the decay rate being quantified in terms of the golden rule.[2] The exploration of atomic autoionization[3] established resonance-continuum inteference effects.[4] A unified conceptual framework applies for these "reactive" nonradiative processes, which involve the decay to a (ionization or dissociation) continuum, and for "nonreactive" radiationless processes involving the coupling and decay to an intramolecular quasicontinuum.[5−15] The theory of nonreactive intramolecular radiationless processes in a bound level structure of large isolated molecules[5−15] focused on electronic−vibrational relaxation (internal conversion and intersystem crossing) and intramolecular vibrational redistribution of electronic-vibrational excitations. Most of the applications of the theory of intramolecular radiationless transitions pertained to the dynamics of intravalence electronic excitations.[5−15] It was also recognized[16−18] that the internal conversion rates of low ($n = 3-5$, where n is the principal quantum number) Rydberg states of large aromatic molecules, i.e., benzene,[19,20] naphthalene,[18−20] and anthracene[21] (as inferred from line broadening), are considerably slower (i.e., by 1−2 orders of magnitude) than those of the intravalence excitations in the same energy domain. The decay channels of low Rydberg states of large molecules below the ionization potential involve both "nonreactive" internal conversion with a partial width $\Gamma_{IC}(n)$ and "reactive" predissociation with a partial width $\Gamma_D(n)$. For Rydbergs above the ionization potential (vibrational and/or rotational and/or spin−orbit induced) autoionization channels with a width $\Gamma_A(n)$ open up. Accordingly,

the lifetime of a Rydberg is expected to be

$$\tau(n) = \hbar/\Gamma(n) \tag{1}$$

where the total width is

$$\Gamma(n) = \Gamma_{IC}(n) + \Gamma_D(n) + \Gamma_A(n) \tag{2}$$

The well-known n^{-3} scaling law,[22,23] which was originally advanced for the radiative decay of atomic Rydbergs[22] and developed for the autoionization of molecular Rydbergs,[23] is expected to hold for all the decay channels, so that the total width of a molecular Rydberg is

$$\Gamma(n) = \Gamma_0/n^3 \tag{3}$$

with the lifetime

$$\tau(n) = (\hbar/\Gamma_0)n^3 \tag{4}$$

where Γ_0 is a numerical constant.

Up to this point we focused on the n dependence of the lifetimes. Regarding the dependence of the energetics and dynamics on the azimuthal quantum number l, two characteristics should be noted. First, the lifetimes are l dependent and eq 4 has to be modified into the form

$$\tau(n,l) = [\hbar/\Gamma_{0(l)}]n^3 \tag{5}$$

where $\Gamma_{0(l)}$ is an l dependent constant. As intramolecular dynamics is manifested in the spatial region close to the nucleus (range A in Fano's terminology),[24,25] the short lifetimes are exhibited for low values of l ($=0-3$). When detailed spectroscopic information on a specific molecular Rydberg series is not available, we shall continue to use eq 4, with the implicit understanding that $\tau(n)$ and Γ_0 refer to a low value of l. Second, the energies of the Rydberg states, which are characterized by the lifetimes (5), are

$$E(n,l) = \text{IP} - \frac{R}{(n - \delta_l)^2} \qquad (6)$$

where R is the Rydberg constant, IP is the ionization potential, and δ_l is the (l-dependent) quantum defect.

The energetics of ultrahigh molecular Rydbergs ($n = 50-300$) were explored by ZEKE (zero-electron kinetic energy) spectroscopy.[26-32] The dynamics of these states (referred to as ZEKE Rydbergs), interrogated by time-resolved ZEKE spectroscopy,[30,33-37] provided compelling evidence for the breakdown of the n^{-3} scaling law, eq 5, which is manifested by the following:

(1) Long lifetimes of ZEKE Rydbergs of NO. Reiser et al.[28] have observed high-lying ($n \gtrsim 100$), very long lived ($\sim\mu$s lifetimes) Rydberg states of NO. Chupka[38,39] has pointed out that the lifetimes of these states are considerably longer than those expected on the basis of the n^{-3} scaling law for the predissociative p series of NO.

(2) Dramatic lifetime lengthening of molecular ZEKE Rydbergs. The lifetimes of ZEKE Rydbergs of large molecules are longer by several (2−4) orders of magnitude than those expected on the basis of the n^{-3} scaling relations.[33] The lifetimes of ZEKE Rydbergs ($n = 80-250$) of bis(benzene)chromimum (BBC) and 1,4-diazabicyclo[2.2.2]octane (DABCO) are longer by 2−3 orders of magnitude than those expected on the basis of eqs 4 and 5.[33]

The fascinating novel characteristics of ZEKE Rydbergs triggered extensive theoretical activity, which falls within the framework of two models:

(A) The Rydberg electron−core rotation model.[33-35,37] This model, which implies the dominance of the (classical) dynamics for the Rydberg electron−core rotation coupling, was discussed elsewhere.[40]

(B) The (l) or (l,m_l) electric field splitting and mixing model. This model was advanced by Bordas et al,[41] Chupka,[38,39] Merkt and Zare,[42] and by us[40] and rests on the following ingredients:

(1) Low l (=0−3) states are active in absorption and in intramolecular relaxation.

(2) Stark splitting and mixing of all the l Rydbergs (with a fixed n) is induced by weak stray electric fields ($F \sim 0.01-0.1$ V/cm) inevitably present in the system or/and by a weak dc background electric field ($F \sim 0.1-1$ V/cm) in the experimental ZEKE setup.

(3) A "democratic" Stark mixing results in the lifetime lengthening for a given manifold, $\tau(n) = (\hbar/\Gamma_0)n^3/D(n)$, where $D(n)$ is the dilution factor. For (l) mixing in a homogeneous electric field,[38-42] $D(n) \sim 1/n$, while for (l,m_l) mixing induced by a homogeneous electric field, in conjunction with the electric field of ions,[42] $D(n) \sim 1/n^2$. For $n = 100$, lengthening of the lifetimes by a huge numerical factor of 10^2-10^4 is expected.

We have drawn[40] on the formal analogy between intramolecular coupling and (interstate and intrastate) relaxation in a bound level structure and the mixing of the components of high Rydbergs in an external electric field. In this paper we shall extend and apply the quantum mechanical mixing model[40] to explore the coupling, accessibility, and decay dynamics of ultrahigh molecular Rydbergs in an external weak (electric field strength $F = 0.01-1.0$ V/cm) electric field.

II. The Dilution

The Stark mixing is formally analogous to intramolecular coupling (Figure 1). The nature and the details of the couplings are qualitatively different. For intramolecular (interstate and intrastate) coupling the doorway state couples in parallel to the entire background manifold and the individual relevant coupling
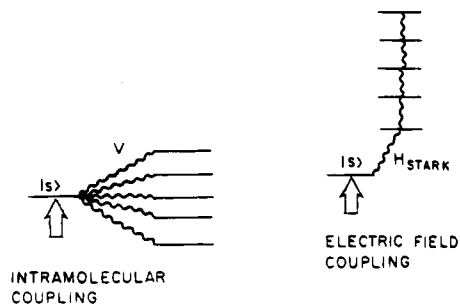
Figure 1. Artist's view of the analogy between interstate coupling in the sparse limit of intramolecular dynamics and field-induced Stark coupling of a Rydberg manifold. $|s\rangle$ denotes the doorway state in both cases.
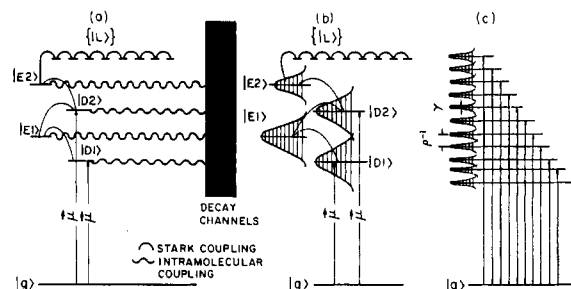
Figure 2. Schematic energy level scene for the splitting and mixing of Rydberg states in an external electric field. (a) Several low-l doorway states $|D1\rangle$ and $|D2\rangle$ and several low-l "pure" escape states $|E1\rangle$, $|E2\rangle$ are separated from the high-l degenerate manifold $\{|L\rangle\}$. The $|D1\rangle$ and $|D2\rangle$ states carry an oscillator strength from the ground state (denoted by a vertical arrow). The $|D1\rangle$, $|D2\rangle$, $|E1\rangle$ and $|E2\rangle$ states are coupled to dissipative continua (predissociation, internal conversion, and/or autoionization channels). The $|D1\rangle$, $|D2\rangle$, $|E1\rangle$ and $|E2\rangle$ states constitute escape states. All the discrete states are sequentially Stark coupled by the (weak) electric field. (b) Stark coupling of the eigenstates of the intramolecular effective Hamiltonian $H_0 - (i/2)\Gamma$. The doorway and "pure" escape states have a partial decay width. The $\{|L\rangle\}$ states in the high-l degenerate manifold have zero decay widths. All the states are coupled by the electric field. (c) Mixed independently decaying levels at a finite field. All these levels carry oscillator strengths for the ground state.

terms are of comparable magnitude.[5-15] On the other hand, for the electric field induced coupling between the zero-order Rydbergs, the coupling is[22] (i) sequential, with $l - (l \pm 1)$ nonvanishing matrix elements, and (ii) hierarchial, with the sequential matrix elements decreasing with increasing l, being proportional to n^2 for low l and being proportional to n for high l. This qualitative difference between intramolecular and Rydberg coupling also results in a difference in the mixed-level structure.

We can now use the arsenal of intramolecular dynamics[5-15] for the Stark (l) coupling and dynamics (Figure 2). (a) The relevant discrete level structure consists of low-l states and a hydrogenic manifold of high-l states. (b) The hydrogenic manifold of high l (>3) will be denoted as $\{|L\rangle|$ states. (c) The few low-l state(s) constitute the doorway state(s) for excitation. The doorway states are determined by the optical excitation conditions, e.g., one-photon excitation, two-photon excitation, or excitation from a metastable intermediate state. (d) The low-l states constitute the escape states for decay. The escape states are coupled to decay channels, i.e., internal conversion, predissociation, and/or autoionization. The distinction between the doorway and escape states constitutes an important feature of the dynamic problem. The doorway state(s) constitute a subset of the escape states. In general, there are $\bar{s}$ doorway states $|Ds\rangle$ ($s = 1- - -\bar{s}$) and $\bar{p} + \bar{s}$ escape states, which consist of $|Ep\rangle$ ($p = 1- - -\bar{p}$) "pure" escape states and the

doorway states $|Ds\rangle$ ($s = 1$- - -$\bar{s}$). The three zero-order manifold consists of the $\{|\kappa\rangle\} \equiv \{|Ds\rangle\}$, $\{|Ep\rangle\}$, and $\{|L\rangle\}$ manifolds (Figure 2).

In the presence of a weak homogeneous electric field F, the Rydberg level structure and dynamics are determined by the effective Hamiltonian[10-15,34]

$$\mathbf{H}_{eff} = \mathbf{H}_0 + \mathbf{H}_{STARK} - (i/2)\,\mathbf{\Gamma} \qquad (7)$$

where $\mathbf{H}_0$ is the diagonal field-free Hamiltonian for the discrete level structure with the energy levels $E(n,l)$, eq 6. $\mathbf{H}_{STARK}$ is the Stark Hamiltonian, with the operator eFz coupling the $\{|\kappa\rangle\}$ states, according to appropriate selection rules. $\mathbf{\Gamma}$ is the decay matrix for the escape states, which also include the doorway state(s). In general, $\mathbf{\Gamma}$ is off-diagonal. The diagonal matrix elements of $\mathbf{\Gamma}$ can be inferred for distinct angular momentum states from the experimental line broadening data for the low-n Rydbergs by using the scaling law (5). Intelligent guesses for the magnitude of the off-diagonal matrix elements of $\mathbf{\Gamma}$ can be obtained from the diagonal matrix elements and invoking appropriate conservation rules, e.g., total angular momentum conservation.

The effective Hamiltonian (7) can be diagonalized by a complex orthogonal transformation, resulting in the independently decaying levels of the system

$$|j\rangle = \sum_{s=1}^{\bar{s}} a_s^{(j)}|Ds\rangle + \sum_{p=1}^{\bar{p}} a_p^{(j)}|Ep\rangle + \sum_L b_L^{(j)}|L\rangle \qquad (8)$$

where $\{a_s^{(j)}\}$, $\{a_p^{(j)}\}$, and $\{b_L^{(j)}\}$ are (complex) coefficients. The (complex) eigenvalues of the system are

$$\epsilon_j = E_j - (i/2)\gamma_j \qquad (9)$$

where E_j are the energy levels and γ_j the decay rates of the molecular eigenstates. (From now on we shall set $\hbar = 1$ in all our equations.) The essential input parameters required for the construction of the effective Hamiltonian at a constant F are (i) the quantum defects δ_s (mod1) and δ_p (mod1) for the $\{|Ds\rangle\}$ and $\{|Ep\rangle\}$ states, respectively, extracted from the Rydberg energetics, and (ii) the width parameters $\Gamma_{0(s)}$ and $\Gamma_{0(p)}$ for the decay width proportionality constants for the $\{(Ds)\}$ and $\{|Ep\rangle\}$ states, respectively, obtained from the line broadening of the lower Rydberg levels. Thus the theory of the dynamics of ultrahigh Rydbergs in weak electric fields rests on the utilization of experimental data. From the point of view of general methodology this approach is similar to the quantum defect method.[24,25]

III. A Simple Model for Field-Induced Mixing

To elucidate some general features of the mixing of dynamics of ultrahigh Rydbergs, we shall represent the doorway and escape state $|s\rangle$ by a single state (characterized by a low value of $l = l_s$ and $m = m_s$) with the energy $E_s = \text{IP} - R/(n - \delta)^2$ and the total nonradiative decay width $\Gamma_s = \Gamma_0/n^3$. At zero field this state is separated from the degenerate hydrogenic manifold of $(n^2 - 1)$ high l, m_l states ($l > l_s$) with the energies $E_l = \text{IP} - R/n^2$ and decay widths $\Gamma_l = 0$, which are not optically accessible from the ground state. The effective Hamiltonian, eq 7, is simplified. $\mathbf{H}_0$ is the (diagonal) field-free Hamiltonian with the energies E_s and $\{E_l\}$. $\mathbf{\Gamma}$ is the decay matrix with the elements Γ_s, $\{\Gamma_l = 0\}$. $\mathbf{H}_{STARK}$ is the Stark Hamiltonian with the operator eFz coupling the doorway state $l_s m_s$ and the states $\{l',m'\}$ with $l' = l_s + 1$, $m' = m_s$, while the states $\{l,m_l\}$ are coupled with $\{l' = l \pm 1, m_l\}$. The independently decaying levels of this model

system are

$$|j\rangle = a_s^{(j)}|s\rangle + \sum_l b_l^{(j)}|l,m_s\rangle \qquad (10)$$

where $a_s^{(j)}$ and $\{b_l^{(j)}\}$ are (complex) coefficients. The (complex) eigenvalues are given by eq 9. The input parameters required for the diagonalization of the effective Hamiltonian (at constant F) are the quantum defect δ (mod1) and the single width parameter Γ_0, which are obtained from experimental data.

At this stage we have obtained all the information on electric field induced mixing within the Rydberg manifold. Of considerable interest is the limit of strong mixing. When the energetic spread of the Stark manifold[22]

$$\Delta W = 6Rn^2(F/5.15 \times 10^9) \qquad (11)$$

(where F is expressed in V/cm) exceeds the zero-field splitting $2\delta R/n^3$ of the doorway state, i.e., $2\delta R/n^3 < \Delta W/2$, the strong mixing of the $|s\rangle$ state with the $\{|l,m_l\rangle\}$ manifold will be realized. The onset of the strong mixing at a fixed n occurs for an electric field

$$F > (3.4 \times 10^5)\delta/n^5 \qquad (12)$$

or, alternatively, the lower limit for the n value where strong mixing prevails is $n_M = 80.5\delta^{1/5}(F/\text{V cm}^{-1})^{-1/5}$. For typical long Rydberg series of large molecules,[33] Even et al found $\delta = 0.41$ for DABCO and $\delta = 1.38$ ($\delta(\text{mod1}) = 0.38$) for BBC, so that for both of these molecular Rydbergs $n_M \simeq 67(F/\text{V} \text{cm}^{-1})^{-1/5}$. In the strong mixing limit for (l) mixing, for $n \geq n_M$ the average lifetime of the diluted states is $\gamma^{-1} \simeq n\tau_s$, where $\tau_s = \hbar/\Gamma_s = \hbar n^3/\Gamma_0$ is the lifetime of the $|s\rangle$ state.

IV. Decay Modes of the Mixed Rydberg Level Structure

We shall be concerned with the optical excitation to and the decay of the mixed level structure, eq 9, of a single high-n (or several high-n) manifold(s) subjected to l mixing. To make contact with real-life situations we consider two experimental observables:[40]

(a) The excited-state total population probability $P(t)$. This corresponds to the time-dependent population of the entire Rydberg manifold. $P(t)$ is interrogated by time-resolved ZEKE spectroscopy by the application of the extracting pulsed electric field at the delay time t after the laser pulse. For a broad-band excitation of a sparse mixed level structure, when $\Delta\omega_p \gg \Delta W$, where $\Delta\omega_p$ is the spectral width of the laser pulse and ΔW is the energetic spread of the Rydberg manifold, eq 20, the population probability is[40]

$$P(t) = \sum_j |a_s^{(j)}|^2 \exp(-\gamma_j t) \qquad (13)$$

exhibiting a superposition of exponentials at all times t. We note that no interference effects (i.e., quantum beats) in the decay are exhibited for $P(t)$.

(b) The population probability $I(t)$ of the doorway state $|s\rangle$. $I(t)$ represents the time-dependent population of the low angular momentum state(s) $|s\rangle$, which is (are) active in absorption. In principle, $I(t)$ could be monitored by time-resolved fluorescence to the ground state, however, the extremely low oscillator strengths (and extremely long radiative lifetimes, i.e., $\propto n^3$) of high Rydbergs preclude this approach. $I(t)$ can be experimentally interrogated by the subsequent photoionization of the Rydberg manifold, with the doorway state being also the active state for ionization. For a broad-band excitation[40]

Ultrahigh Rydbergs in Weak Electric Fields

J. Phys. Chem., Vol. 99, No. 19, 1995 **7469**

$$I(t) = \sum_j |a_s^{(j)}|^4 \exp(-\gamma_j t) +$$

$$\sum_j \sum_{j'} |a_s^{(j)}|^2 |a_s^{(j')}|^2 \exp[i(E_j - E_{j'})] \exp[-(\gamma_j + \gamma_{j'})t/2] \quad (14)$$

consisting of direct decay terms and of oscillatory interference terms. The latter exhibit quantum beats, i.e., temporal coherence effects.

As is known from the theory of intramolecular dynamics,[5-15] the total decay probability, eq 13, involves only direct exponential decay terms, while quantum beats can be manifested in the decay of a specific wavepacket of states (i.e., a subspace of the discrete Hilbert space), such as the decay of the doorway state, eq 14.

All the available experimental information on the dynamics of ultrahigh Rydbergs emerges from time-resolved ZEKE experiments. These experiments are performed by using conventional nanosecond lasers with $\Delta\omega_p = 0.1-0.5$ cm^{-1}. To characterize the experimental conditions we take for eq 11 $\Delta W = 1.3 \times 10^{-4} n^2(F/V$ cm$^{-1})$ and obtain $\Delta W = 0.13$ cm^{-1} for $n = 100$ at $F = 0.1$ V/cm. Accordingly, $\Delta\omega_p \gtrsim \Delta W$, whereupon the broad band excitation will be accomplished under ns excitation. The population decay $P(t)$ is expected to be given by eq 13. The decay will not be exponential, reflecting the distribution of the decay lifetimes for a fixed external field.

V. Field-Induced Mixing within a Single Rydberg Manifold

To explore the general features of field-induced (l) mixing, we consider the dilution within the high Rydbergs of the DABCO molecule, which was studied by Even et al.[33] The $n = 10-30$ Rydbergs of DABCO[33] exhibit three series. The prominent Rydberg series, with the largest quantum defect, is tentatively assigned to the s ($l = 0$) series.[33] This prominent Rydberg series is characterized by the parameters[33]

$$\delta = 0.41 \quad \Gamma_0 = 3 \times 10^3 \text{ cm}^{-1} \quad (15)$$

for the quantum defect and the decay widths, respectively. We shall take a single doorway state for each n, which is characterized by the parameters in eq 15. This single doorway state, taken as $|s\rangle = |l = 0, m_l = 0\rangle$, is mixed by hierarchial and sequential Stark coupling with the inactive manifold $\{|l,m_l=0\rangle\}$. It will be also useful to specify the homogeneous electric field in terms of reduced units, i.e.,

$$\bar{F} = (F/V \text{ cm}^{-1})n^5/(3.4 \times 10^9)\delta \quad (16)$$

For $\bar{F} = 0$ the isolated $|s\rangle$ resonance is characterized by the lifetime

$$\tau_s = \hbar/\Gamma_s = \hbar n^3/\Gamma_0 \quad (17)$$

The diagonalization of the effective Hamiltonian, eq 7, for fixed values of n, δ, Γ_s, and F, results in the following relevant parameters: (i) the energies E_j, (ii) the lifetimes $\tau_j = \hbar/\gamma_j$, and (iii) the mixing coefficients of the doorway state $|a_s^{(j)}|^2$. From these data we have constructed the lifetime spectra (τ_j vs E_j), the accessibility spectra ($|a_j^{(s)}|^2$ vs E_j), and the lifetime-accessibility maps ($|a_j^{(s)}|^2$ vs τ_j).

Model calculations were performed for $n = 50$ and $n = 100$ manifolds of DABCO. In Figure 3 we present the lifetime spectra and the accessibility spectra for $n = 50$ at $F = 10$ V/cm ($\bar{F} = 2.1$), while a typical lifetime-accessibility map for $n = 50$ at $F = 20$ V/cm ($\bar{F} = 4.2$) is portrayed in Figure 4. The lowest
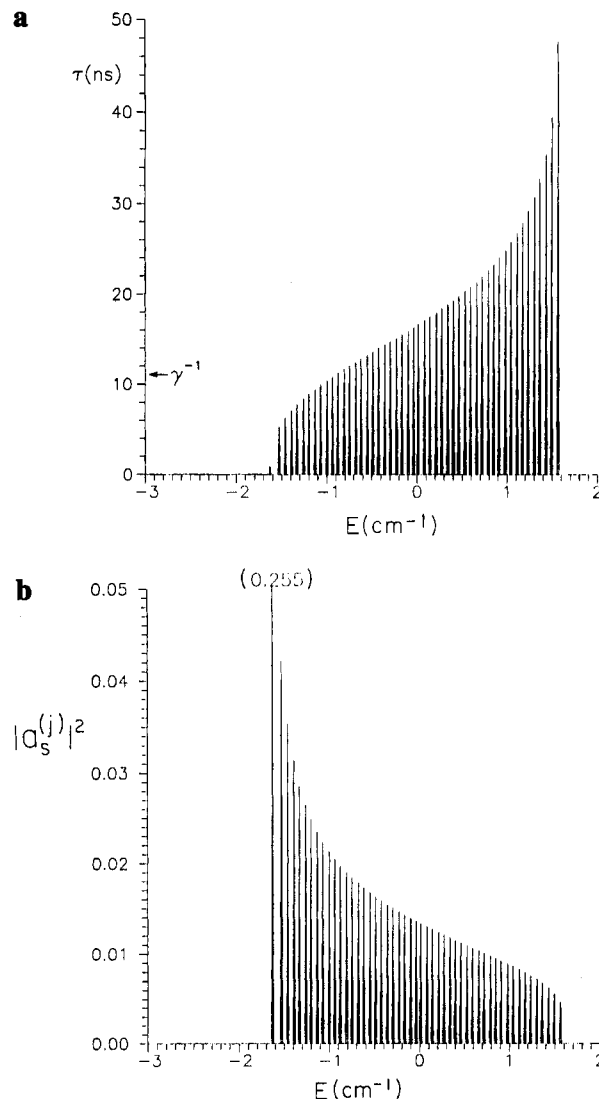
Figure 3. Lifetime and accessibility spectra for the $n = 50$ Rydberg manifold of DABCO for $F = 10$ V/cm ($\bar{F} = 2.1$). (a) The lifetime spectrum (τ_j vs E_j). Note the lowest energy shortest lifetime $\tau_1 = 0.3$ ns. The average diluted lifetime $\gamma^{-1} = n\tau_s = 11$ ns is marked by an arrow. (b) The accessibility spectrum ($|a_s^{(j)}|^2$ vs E_j). The amplitude of the doorway state in the lowest energy, shortest lifetime state is $|a_s^{(1)}|^2 = 0.255$.

energy, short lifetime (Figure 3a) of $\tau_1 = 0.3$ ns is close to and slightly longer than the value of $\tau_s = 0.22$ ns, eq 17, with a weight (Figure 3b) of $|a_s^{(1)}|^2 = 0.26$. This short lifetime corresponds to the residue of the doorway state. The distribution of the longer lifetimes (Figures 3a and 4) represents the diluted states. The lifetime and amplitude spectra are asymmetric, with τ_j inreasing at higher energies (Figure 3a), while $|a_s^{(j)}|^2$ decreases with increasing energy (Figure 3b). Consequently, the lifetime-accessibility spectrum is also asymmetric with longer lifetimes being characterized by smaller amplitudes (Figure 4). These features manifest the effects of the sequential Stark coupling. The average value of $\gamma^{-1} = n\tau_s = 11$ ns falls in the middle of the asymmetric distribution.

VI. The Hierarchy of the Two Time Scales

To provide a physical picture of the evolution of the field-induced mixing with increasing F, we present in Figure 5 the lifetime-accessibility maps (plotted as $|a_s^{(j)}|^2$ vs the decay widths γ_j) of $n = 100$ for $F = 0.1$ V/cm ($\bar{F} = 0.72$), 0.2 V/cm ($\bar{F} = 1.44$), and 0.3 V/cm ($\bar{F} = 2.2$). The lifetime of the doorway

7470 *J. Phys. Chem., Vol. 99, No. 19, 1995*

Bixon and Jortner
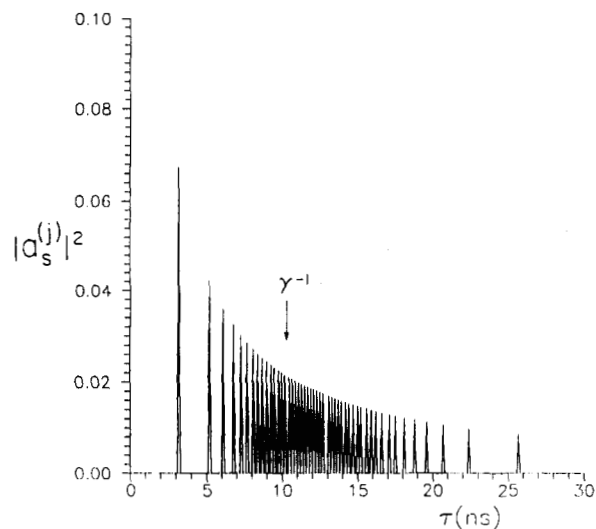
Figure 4. Lifetime-accessibility map for the $n = 50$ Rydberg manifold of DABCO for $F = 20$ V/cm ($\bar{F} = 4.2$). The contributions of the long lifetimes ($j \neq 1$) are presented. The average diluted lifetime $\gamma^{-1} = n\tau_s = 11$ ns is marked by an arrow.
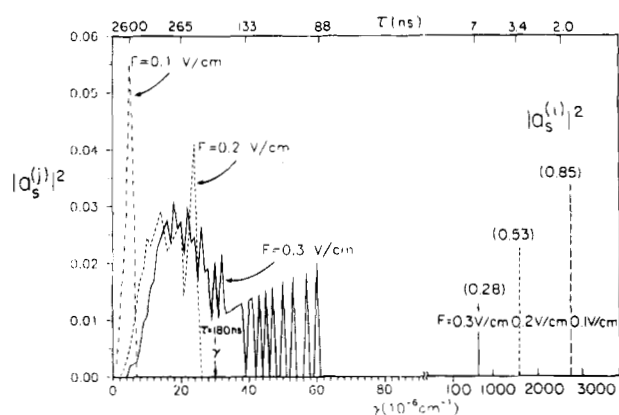
Figure 5. Lifetime-accessibility maps for the $n = 100$ Rydberg manifolds of DABCO for $F = 0.1$, 0.2, and 0.3 V/cm. Note the two distinct time scales. The short lifetimes are specified by the amplitudes $|a_s^{(1)}|^2$ (in brackets). The long lifetimes exhibit a broad distribution. The average diluted lifetime $\tau = n\tau_s = 180$ ns (marked by an arrow) provides a reasonable mean value for the distribution at $F = 0.3$ V/cm ($\bar{F} = 2.2$).

state is $\tau_s = 1.8$ ns. These $\bar{F}$ values span the range from weak coupling toward strong coupling. These results exhibit the following features:

(1) Two distinct time scales for the decay.

(2) A short lifetime τ_{SHORT} which appears in the range $\tau_{SHORT} = 2.0-7.0$ ns. These short decay times represent the residue of the doorway state, as is evident from the decrease of their amplitude $|a_s^{(1)}|^2$ with increasing $\bar{F}$ (Figure 5). τ_{SHORT} for low $\bar{F}$ is close to τ_s, while with increasing $\bar{F}$, τ_{SHORT} becomes longer.

(3) A broad distribution of long decay times $\{\tau_{LONG}\}$. This distribution of the lifetimes corresponds to the diluted states, which have parentage in the inactive $l \neq 0$ manifold. For weak mixing ($\bar{F} = 0.72$) the distribution of these long lifetimes is rather narrow with a maximum in the microsecond time range. With increasing $\bar{F}$ this distribution becomes broader. At $\bar{F} = 2.2$, which approaches the strong mixing limit, a broad distribution around the mean value of $\gamma^{-1} = n\tau_s = 180$ ns is exhibited.

In Figure 6 we portray the time evolution of the total population $P(t)$, eq 13. $P(t)$ exhibits a bimodal population decay, which is distinct from dephasing, being characterized by two
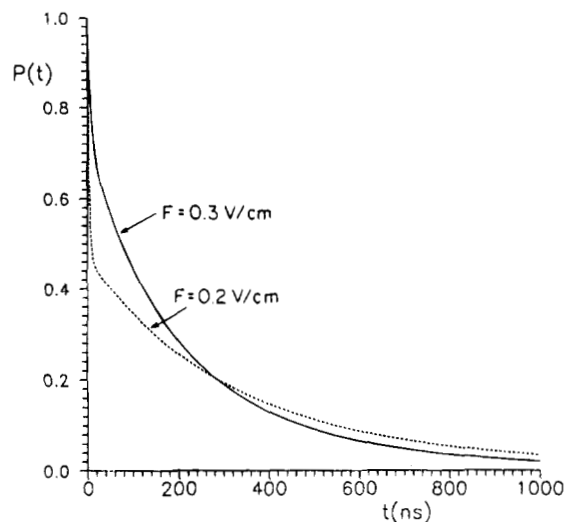
Figure 6. Time-resolved total population of the $n = 100$ manifold of DABCO at $F = 0.2$ V/cm and at $F = 0.3$ V/cm.
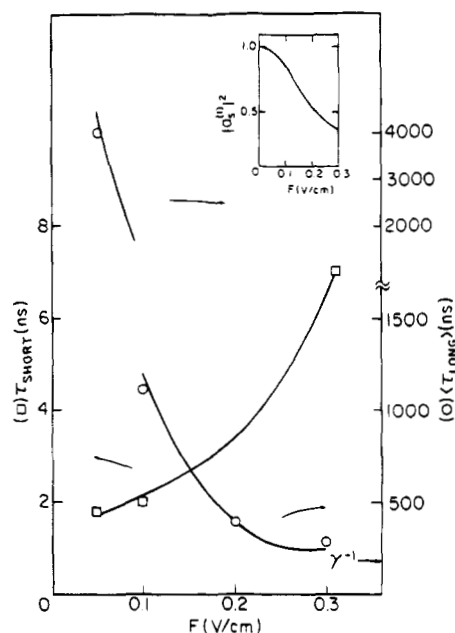
Figure 7. Electric-field dependence of the short lifetime τ_{SHORT} and of the average long lifetime $\langle\tau_{LONG}\rangle$ for the $n = 100$ manifold of DABCO. The insert shows the electric-field dependence of the weight $|a_s^{(1)}|^2$ of the doorway state within the lowest energy eigenstate. The solid lines represent the description of τ_{SHORT} by eq 18 and of $\langle\tau_{LONG}\rangle$ by eq 19.

time scales: range (I), the short lifetime τ_{SHORT}; range (II), the distribution of long lifetimes $\{\tau_{LONG}\}$ with the average value $\langle\tau_{LONG}\rangle$.

To provide a reasonable approximate description of the electric field dependence of the decay lifetimes, we consider their dependence on the weight $|a_s^{(1)}|^2$ of the lower energy eigenstates, i.e., the residue of the doorway state. In Figure 7 we present the electric field dependence of the short lifetime τ_{SHORT} and of the averaged value of the long lifetime $\langle\tau_{LONG}\rangle$. τ_{SHORT} is well represented by

$$\tau_{SHORT} \simeq \tau_s/|a_s^{(1)}|^2 \tag{18}$$

For a broad distribution of the long lifetimes a crude approximation for the mean value is

$$\langle\tau_{LONG}\rangle \simeq n\tau_s/(1 - |a_s^{(1)}|^2) \tag{19}$$

Ultrahigh Rydbergs in Weak Electric Fields

J. Phys. Chem., Vol. 99, No. 19, 1995 **7471**

As is evident from Figure 7, eqs 18 and 19 provide a good description of the time scales of decay times.

The total population probability in the weak mixing regime is approximately given by the superposition of the contributions from the two time domains, in the form

$$P(t) \simeq |a_s^{(1)}|^2 \exp(-t/\tau_{SHORT}) +$$
$$(1 - |a_s^{(1)}|^2) \exp(-t/\langle\tau_{LONG}\rangle) \quad (20)$$

With the increase of $\bar{F}$ above $\bar{F} > 1$, we expect that in range I, τ_{SHORT} increases (toward $n\tau_s$) and the amplitude $|a_s^{(1)}|^2$ of the short component decreases, while in range II the average diluted value of $\langle\tau_{LONG}\rangle$ tends toward $n\tau_s$. The strong mixing limit is realized for $\bar{F} > 1$ with $|a_s^{(1)}|^2 \rightarrow 1/n$, τ_{SHORT}, $\langle\tau_{LONG}\rangle$ $\rightarrow n\tau_s$. The contribution of range I to $P(t)$, eq 20, becomes small and indistinguishable from that of range II, which provides the dominating contribution to $P(t)$ with the mean lifetime $\tau_s/D(n)$. This heuristic, but physical, description predicts that (1) two distinct ($\sim$ns and $\sim\mu$s) time scales for the dynamics for $\bar{F} < 1$ will be exhibited, (2) the lengthening of the short (ns) temporal decay component with increasing $\bar{F}$ is expected for $\bar{F} \lesssim 1$, (3) a broad distribution of long lifetimes with the average value of $\simeq(10-20)n\tau_s$, i.e., in the microsecond time domain, is expected for $\bar{F} < 1$, (4) the long lifetimes exhibit a broad distribution, (5) the average long lifetime decreases with increasing $\bar{F}$, (6) coalescence of the lifetimes toward the mean diluted lifetime $n\tau_s$ occurs in the strong mixing limit ($\bar{F} > 1$).

These predictions for the novel and rich dynamics in the weak mixing ($\bar{F} < 1$) domain provide guidelines for the understanding of experimental data. In particular, our analysis provides clues for (a) the possibility of observation of extremely long ($\sim$ a few microseconds) lifetimes of ZEKE Rydbergs,[28-31] (b) pronounced nonexponentiality of the long-time decay of ZEKE Rydbergs,[33,34] and (c) the dramatic (2-3 orders of magnitude) break in the Rydberg lifetimes vs n^3 corresponds to the "transition" from range I to range II, which occurs at $n \simeq n_M$ ($\bar{F} \sim 1$), when the contribution of range II to the decay dynamics becomes dominant.

The central prediction for the occurrence of two distinct time scales for the dynamics of Rydbergs ($\bar{F} < 1$) was not yet verified experimentally. Our predictions have to be verified by the extension of the time-resolved ZEKE technique into the time domain of 1-10 ns.

VII. Mixing of Several Rydberg Manifolds

Up to this point we have focused on field-induced mixing within a single Rydberg (n) manifold. The mixing between neighboring n manifolds is negligible provided that $\bar{F} < 1/\delta$. Accordingly, for the DABCO model molecule with $\delta = 0.41$, the mixing within a single manifold constitutes a proper picture for $\bar{F} < 2.5$. Thus, our treatment in the preceding section (VI) of a single $n = 100$ manifold with $\delta = 0.41$ in the range of electric-field strength $\bar{F} = 0.72-2.2$ is valid. For $\bar{F} > 2.5$ the mixing within several neighboring manifolds with consecutive n values has to be considered. The intermanifold n mixing for the DABCO model molecule now involves the Stark coupling of several doorway (and escape) states, i.e., $|n,l=0\rangle$, of different n with the corresponding inactive, i.e., $\{|n,l\neq0\rangle\}$, manifolds of distinct n values. The independently decaying levels obtained from the diagonalization of the effective Hamiltonian with $\bar{s}$ doorway (and escape) zero-order states $|n,l=0\rangle$, with consecutive n, are given by eq 8 with all $a_p^{(j)} = 0$. The excited-state total population probability, eq 13, is extended to be
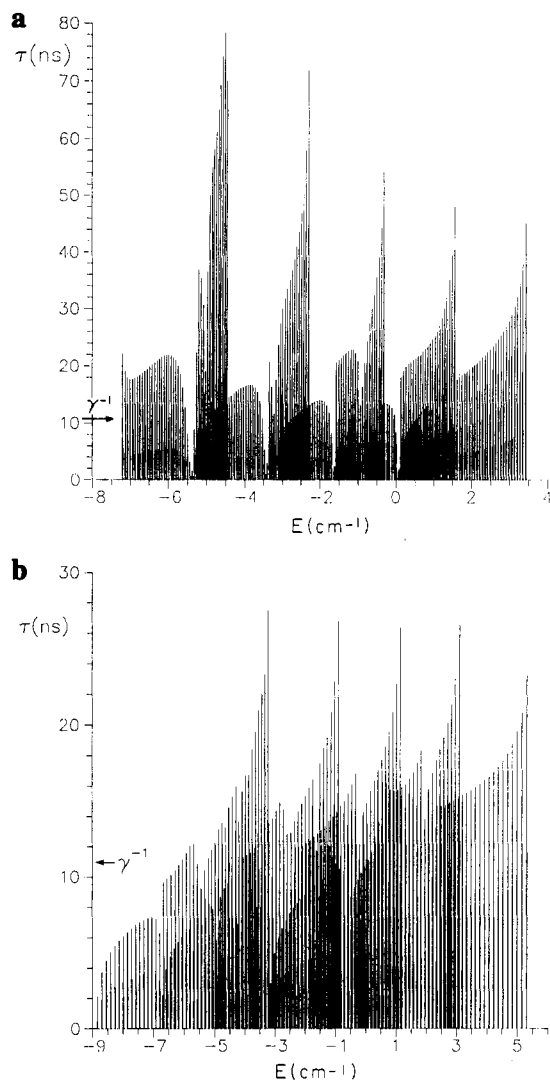
Figure 8. Lifetime spectra for the $n = 51-50-49-48-47$ mixed Rydberg manifold of DABCO at different electric fields. (a) $F = 10$ V/cm ($\bar{F} = 2.1$). This situation corresponds to $\bar{F} \lesssim 1/\delta$. The average lifetime $\gamma^{-1} = n\tau_s = 1$ ns is marked by an arrow. (b) $F = 20$ V/cm ($\bar{F} = 4.2$). This situation corresponds to strong intermanifold mixing $\bar{F} > 1/\delta$. The average lifetime $\gamma^{-1} = n\tau_s = 11$ ns is marked by an arrow.

$$P(t) = \sum_j |\sum_{s=1}^{\bar{s}} a_s^{(j)}|^2 \exp(-\gamma_j t) \quad (21)$$

In Figure 8 we present the results of model calculations for the mixing of several n manifolds of DABCO in the vicinity of $n = 50$, incorporating five manifolds with $n = 47-51$. The lifetime spectra are shown for $F = 10$ V/cm ($\bar{F} = 2.1$, i.e., $\bar{F} \simeq 1/\delta$), on the verge of effective intermanifold n mixing (Figure 8a) and for $F = 20$ V/cm ($\bar{F} = 4.2$, i.e., $\bar{F} > 1/\delta$), where intermanifold n mixing is extensive, i.e., $\bar{F} > 1/\delta$ (Figure 8b).

For $\bar{F} \simeq 1/\delta$ (Figure 8a) the overall appearance of the spectrum is characterized by a superposition of the spectra for distinct n values (as is the case for $\bar{F} \ll 1/\delta$). The onset of overlap between neighboring n manifolds is manifested by destructive interference effects exhibiting "holes" in the lifetime spectra (Figure 8a), which can be rationalized by the amplitude sums in eq 21. With a further increase of $\bar{F}$ above $1/\delta$ (Figure 8b), overlap between manifolds is extensive. In the middle energy range of the lifetime spectrum for effective intermanifold mixing (Figure 8b), the regularity of the lifetimes and the accessibility spectra for a single manifold (see Figure 3) are
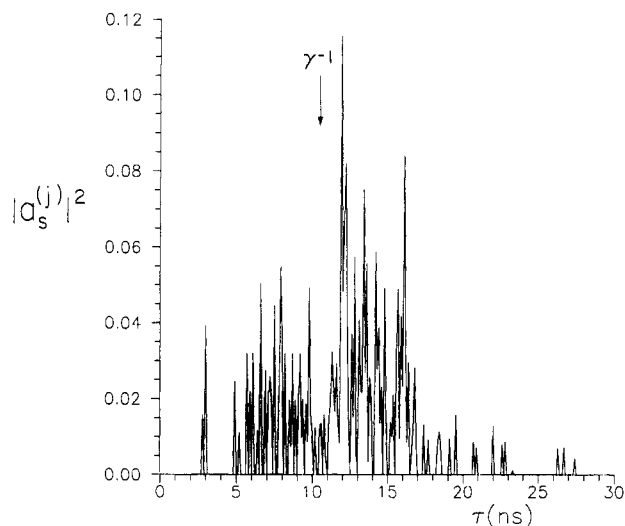
Figure 9. Lifetime-accessibility map for the central energy part of the $n = 51-50-49-48-47$ mixed Rydberg manifold (in the energy range $E = -1.5$ to 1.5 cm^{-1}) of DABCO for $F = 20$ V/cm ($\bar{F} = 4.2$). The average lifetime $\gamma^{-1} = n\tau_s = 11$ ns is marked by an arrow.

smeared out (Figure 8b). For the strong field mixing ($\bar{F} \gg 1$) and effective intermanifold mixing ($\bar{F} \gg 1/\delta$), the lifetime-accessibility maps for a middle value of n (Figure 9) are considerably more irregular than the regular asymmetric distribution for the single n manifold. This conclusion is apparent from the comparison between Figure 4 (for a single $n = 50$) and Figure 9 (for five $n = 47-51$ manifolds) at $F = 20$ V/cm ($\bar{F} = 4.2$). In spite of the difference in the details of the maps for a single n and for several n values, the gross features of the maps in Figures 4 and 9 are similar. Both for single n and several n effective mixing (Figures 4 and 9), the average values of $\gamma^{-1} = n\tau_s = 11$ ns (for $n = 50$) fall in the middle of the distribution, whose lifetime spread is similar in both cases. Accordingly, the time-resolved decay is expected to be similar for the strongly mixed single n and multi n manifolds.

VIII. Concluding Remarks

We have provided a physical picture for the dynamics of ultrahigh Rydbergs in an external (homogeneous) electric field, which bears a close analogy to intramolecular dynamics. From the technical point of view the picture of the dynamics of ultrahigh Rydbergs has to be, and was,[43] extended to include the effects of overall features of multichannel mixing. The simple picture, which rests on a single l (e.g., $l = 0$) doorway and escape state(s) with a decay width Γ_0/n^3, has to be extended. Several low-l states ($l = 0-3$), each characterized by a distinct quantum defect δ_l and a decay width $\Gamma_0(l)/n^3$, have to be incorporated in the effective Hamiltonian, eq 7. In some cases, when several of these low-l states decay to a common channel, the decay matrix $i\Gamma/2$ in eq 7 is nondiagonal. The accessibility of the doorway state(s) is determined by the specific, e.g., one-photon or two-photon, excitation conditions. Multichannel coupling quantitatively modifies the level mixing and the effect of the external weak electric field on the time-resolved decay, as we have found for the dynamics of the Rydbergs of NO.[43]

From the point of view of general methodology, we have focused on the dynamics of ultrahigh mixed Rydberg manifolds. Our analysis provides a universality principle for a unified description of the level structure and dynamics of high Rydbergs of molecules and of autoionizing atoms. This universality principle was borne out by the experimental observation by the lifetime lengthening of high ($n \geq 100$) autoionizing ZEKE

Rydberg states of Ar, i.e., the $^3P_{1/2}ns'[1/2]_1$ and $^2P_{1/2}nd'[3/2]_1$ series studied by Merkt[44] and the $^2P_{1/2}np'[3/2]_1$ series studied by Even,[45] which were theoretically explored[43] by the multichannel effective Hamiltonian formalism.

References and Notes

(1) Bonhoeffer, K. F.; Farkas, L. Z. Phys. Chem., 1928, 134, 337.
(2) Wenzel, G. Z. Phys. 1928, 29, 321.
(3) Beutler, H. Z. Phys. 1933, 86, 710.
(4) Fano, U. Nuovo Cimento 1935, 12, 156.
(5) Bixon, M.; Jortner, J. J. Chem. Phys. 1968, 48, 715.
(6) Bixon, M.; Jortner, J. Mol. Cryst. 1969, 213, 237.
(7) Bixon, M.; Jortner, J. Isr. J. Chem. 1969, 1, 189.
(8) Bixon, M.; Jortner, J. J. Chem. Phys. 1969, 50, 3284.
(9) Bixon, M.; Jortner, J. J. Chem. Phys. 1969, 50, 4061.
(10) Bixon, M.; Dothan, Y.; Jortner, J. Mol. Phys. 1969, 17, 109.
(11) Mukamel, S.; Jortner, J. In The World of Quantum Chemistry; Daudel, R., Pullman, B., Eds.; Proc. First Intl. Congress Quantum Chemistry; Menton, France 1973; D. Reidel Publ. Co., 1974; pp 145–109.
(12) Mukamel, S.; Jortner, J. In MTP International Review of Science; Buckingham, A. D., Coulson, C. A., Eds.; London: Butterworth, 1976; Vol. 13, p 327.
(13) Mukamel, S.; Jortner, J. In Excited States; Lim, E. C., Ed.; Academic Press: New York, 1977; Vol. III, pp 57–107.
(14) Kommandeur, J.; Jortner, J. Chem. Phys. 1978, 28, 273.
(15) Levine, R. D.; Jortner, J. In Advances in Chemical Physics; Jortner, J., Levine, R. D., Rice, S. A., Eds.; Wiley: New York, 1981; Vol. 47, pp 1–114.
(16) Jortner, J. J. Chim. Phys. Special Issue. Transitions Non Radiatives Dans Les Molécules, 1969, 9.
(17) Jortner, J.; Leach, S. J. Chim. Phys. 1980, 77, 7. Jortner, J.; Leach, S. J. Chim. Phys. 1980, 77, 43.
(18) Jortner, J.; Morris, G. C. J. Chem. Phys. 1969, 51, 3689.
(19) Whetten, R. L.; Grubb, S. G.; Otis, C. E.; Albrecht, A. C.; Grant, E. R. J. Chem. Phys. 1985, 82, 1115.
(20) Amirav, A.; Jortner, J. J. Chem. Phys. 1985, 82, 4378.
(21) Amirav, A.; Jortner, J., unpublished results.
(22) Bethe, H. A.; Salpeter, E. E. Quantum Mechanics of One- and Two-Electron Atoms; Springer Verlag: Berlin, 1957.
(23) (a) Berry, R. S. J. Chem. Phys. 1966, 45, 1228. (b) Bradsley, N. Chem. Phys. Lett. 1967, 1, 229.
(24) Fano, U. Phys. Rev. A 1970, 2, 353.
(25) Fano, U. Opt. Soc. Am. 1975, 65, 979.
(26) Müller-Dethlefs, K.; Sander, M.; Schlag, E. W. Chem. Phys. Lett. 1984, 112, 291.
(27) Müller-Dethlefs, K.; Sander, M.; Schlag, E. W. Z. Naturforch. 1984, 38A, 1089.
(28) Reiser, G.; Habenicht, W.; Müller-Dethlefs, K.; Schlag, E. W. Chem. Phys. Lett. 1988, 152, 119.
(29) Müller-Dethlefs, K.; Schlag, E. W. Annu. Rev. Phys. Chem. 1991, 42, 109.
(30) Scherzer, W. G.; Selzler, H. L.; Schlag, E. W.; Levine, R. D. Phys. Rev. Lett. 1994, 72, 1435.
(31) Scherzer, W. G.; Selzler, H. L.; Schlag, E. W. Z. Naturforsch. 1993, 48A, 1256.
(32) Merkt, F.; Softley, T. P. Int. Rev. Phys. Chem. 1993, 12, 205.
(33) Even, U.; Levine, R. D.; Bersohn, R. J. Phys. Chem. 1994, 98, 3472.
(34) Bahatt, D.; Even, U.; Levine, R. D. J. Chem. Phys. 1993, 98, 1744.
(35) Even, U.; Ben-Nun, M.; Levine, R. D. Chem. Phys. Lett. 1993, 210, 416.
(36) Merkt, F. J. Chem. Phys. 1994, 100, 2623.
(37) Rabani, E.; Baranov, L. Ya.; Levine, R. D.; Even, U. Chem. Phys. Lett. 1994, 221, 473.
(38) Chupka, W. A. J. Chem. Phys. 1993, 98, 4520.
(39) Chupka, W. A. J. Chem. Phys. 1993, 99, 5800.
(40) Jortner, J.; Bixon, M. J. Chem. Phys., in press.
(41) Bordas, C.; Brevet, P. F.; Broyer, M.; Chevaleyre, J.; Labastie, P.; Perrot, J. P. Phys. Rev. Lett. 1988, 60, 917.
(42) Merkt, F.; Zare, R. N. J. Chem. Phys. 101, 101, 3495.
(43) Bixon, M.; Jortner, J., to be published.
(44) Merkt, F. J. Chem. Phys. 1994, 100, 2623.
(45) Even, U., to be published.